Discrete transparent boundary conditions for the Schrödinger equation – a compact higher order scheme

Maike Schulte*, Anton Arnold†

September 27, 2007

We consider the two-dimensional time-dependent Schrödinger equation with the new compact nine-point scheme in space and the Crank-Nicolson difference scheme in time. For the resulting difference equation we derive discrete transparent boundary conditions in order to get highly accurate solutions for open boundary problems. Numerical experiments illustrate the perfect absorption of outgoing wave independently of their impact angle at the boundary. Finally, we apply inhomogeneous discrete transparent boundary conditions to the transient simulation of quantum waveguides.

1 Introduction

The development of novel semiconductor devices (like diodes or transistors) is usually supported by computer simulations to optimize the desired operating features. Schrödinger models describe the purely ballistic transport of electrons and holes, and they are employed for simulations of quantum waveguides and nano-scale semiconductor heterostructures, e.g. The time-dependent two-dimensional Schrödinger equation

*Institut für Angewandte und Numerische Mathematik, Westfälische Wilhelms-Universität Münster, Einsteinstr. 62, D-48149 Münster, Germany, Maike.Schulte@math.uni-muenster.de

†Institut für Analysis und Scientific Computing, Technische Universität Wien, Wiedner Hauptstr. 8, A-1040 Wien, Austria, Anton.Arnold@tuwien.ac.at

describes the time evolution of the complex-valued wave function ψ. It reads

$$\begin{aligned} i\frac{\partial}{\partial t}\psi(x,y,t) &= -\frac{1}{2}\Delta\psi(x,y,t) + V(x,y,t)\psi(x,y,t), \quad (x,y) \in \Omega \subset \mathbb{R}^2,\ t > 0, \\ \psi(x,y,0) &= \psi^I(x,y) \in L^2(\Omega), \end{aligned} \tag{1.1}$$

with the real-valued potential $V(x,y,t)$.

As in [ArEhSo03], we assume that Ω is an infinitely long stripe, i.e. $\Omega = \mathbb{R} \times (0,Y)$, with ψ satisfying homogeneous Dirichlet boundary conditions at $y = 0$ and $y = Y$. For computational purposes it is necessary to reduce the simulations to some finite subdomain, say $\Omega_{comp} := (0,X) \times (0,Y) \subset \Omega$ by introducing (artificial) open boundary conditions at $x = 0$ and $x = X$. As it is common practice, we assume *supp* $\psi^I \subset \Omega_{comp}$, and that the potential is constant in the two exterior domains $\mathbb{R}^- \times (0,Y)$ and $(X,\infty) \times (0,Y)$. Note that an only time-dependent exterior potential can be dealt with by the transformation $\psi(x,t) = \varphi(x,t) \exp\left[\int_o^t V(\tau)d\tau\right]$.

Open boundary conditions are called *transparent*, if they yield identical solutions both on the original large domain Ω and the reduced domain Ω_{comp}. In the 1D case the transparent boundary condition (TBC) takes the form

$$\frac{\partial}{\partial \eta}\psi = -\sqrt{2}e^{-i\pi/4}e^{-iV_{ext}t}\sqrt{\partial_t}\left(e^{iV_{ext}t}\psi\right), \qquad x = 0 \text{ or } x = X, \tag{1.2}$$

where η denotes the unit outward normal vector at each interface and V_{ext} is the constant exterior potential. $\sqrt{\partial_t}$ is the fractional time derivative of order $\frac{1}{2}$ with the Fourier symbol $\sqrt{-i\omega}$, and it can be rewritten as a time-convolution of the boundary data:

$$(\sqrt{\partial_t}\psi)(x,t) = \frac{1}{\sqrt{\pi}}\frac{d}{dt}\int_0^t \frac{\psi(x,\tau)}{\sqrt{t-\tau}}d\tau\,. \tag{1.3}$$

When carrying out the t-derivative, one sees that the resulting kernel behaves like $\mathcal{O}(t^{-3/2})$ for $t \to \infty$. The one dimensional TBC (1.2) has been derived by several authors, e.g. in [BaPo91], [Pa82]. Its extension to rectangular geometries in 2D is based on taking the partial Fourier series of ψ w.r.t. y:

$$\psi(x,y,t) = \sum_{m\in\mathbb{N}} \hat{\psi}_m(x,t)\sin\left(\frac{m\pi y}{Y}\right).$$

Since V is constant in each of the two exterior domains, the time evolution of the modes $\hat{\psi}_m(x,t)$, $m \in \mathbb{N}$ is decoupled there. Hence, each mode satisfies at $x = 0$ and $x = X$ a 1D TBC:

$$\frac{\partial}{\partial \eta}\hat{\psi}_m(x,t) = -\sqrt{2}e^{-\pi/4}e^{-iV_m t}\sqrt{\partial_t}\left(e^{iV_m t}\hat{\psi}_m(x,t)\right), \qquad m \in \mathbb{N}, \tag{1.4}$$

with the potentials $V_m := V_{ext} + \frac{1}{2}\left(\frac{m\pi}{Y}\right)^2$.

The goal of this paper is to derive and analyze a discrete analogue of (1.4) in conjunction with a fourth order finite difference scheme of the Schrödinger equation. Discretizations of TBCs are delicate even in the 1D case, as they may lead to unphysical reflections at the boundaries (cf. [BaPo91], [Ma89], [Sc02]). Here we shall follow the "philosophy" of [Ar98], [EhAr01], [ArEhSo03] and derive *discrete transparent boundary conditions* (DTBCs), instead of discretizing the analytic TBC (1.4). We shall now first review several popular discretization schemes for the Schrödinger equation as well as existing strategies for treating absorbing boundary conditions (ABCs) for it. ABCs are *local* approximations to the exact, but *nonlocal* TBC (1.2).

A popular spatial discretization of the Schrödinger equation is based on the second order finite difference scheme. Together with a Crank-Nicolson scheme in time, this yields an unconditionally stable scheme. In many applications compact higher order finite difference schemes are used (e.g. the fourth order *Numerov scheme*, cf. [KaMoSi05], [Mo04]). And this will be the starting point for this paper. Another approach is given in [BaShMa02], where a time-splitting spectral approximation is developed for the Schrödinger equation. This strategy is very efficient for smooth solutions, but has no advantage for heterostructures (with discontinuous potentials), since the potential is assumed to be periodic in space and $C^\infty(\mathbb{R})$ in [BaShMa02]. In [BoDe06] Borzi and Decker combined a pseudospectral method for the space discretization with a leap-frog time-propagation scheme, which is second order accurate in time and yields spectral accuracy in space.

The simplest possibility to implement ABCs for Schrödinger-type equations is to enlarge the computational domain and to add some complex-valued potential just outside the domain of interest in order to damp the solution there. This approach was first presented in [KoKo86], [NeBa89] and is also often used in physical applications (e. g. [Bu97], [HePfSt07]). However, it only works well for one tunable wavenumber of the wavefunction ψ. Pseudodifferential techniques, like in the seminal works of Engquist and Majda in [EnMa77], [EnMa79] for the wave equation have been used by Shibata [Sh91] and Kuska [Ku92]. Since their analytical approaches lead to non-local (in time) boundary conditions (cf. (1.2)), they used approximations of the square root symbol by low order rational functions. In [Fe99] Fevens and Jiang derived ABCs for the Schrödinger equation which depend on the group velocity of the travelling wave package. Only the parts with a positive velocity are admitted to pass the right boundary. But the discretization of these ABCs leads to weakly ill-posed problems, as shown in [AlRe02]. Furthermore, one has to know the (main) velocity of the solution a-priori. So, these ABCs are not practical either. In [AlRe04] Alonso-Mallo and Reguera calculated ABCs for the semidiscrete Schrödinger equation in space, the fully discrete model is described in [AlRe03]. Both approaches are weakly unstable and show increasing instabilities for higher order ABCs. In [AnBe01] Antoine and Besse derived ABCs on a curved artificial boundary. Their well-posedness and discretization is studied in [AnBeMo04]. A gener-

alization of the 2D-result of Antoine and Besse is formulated by Szeftel in [Sz04A] for both linear and non-linear Schrödinger equations in $\mathbb{R}^d$. Here, the author used also a pseudodifferential approach and obtained the boundary operator based on a reflection-of-singularities-theory for the Schrödinger equation (cf. [Sz04B]). In order to get local ABCs both in space and time, he adapted the approximation strategy from [EnMa79]. The results are good for the linear case, but poor in the non-linear case. For a more detailed review of ABCs and TBCs we refer to [AABES07].

Exact DTBCs were developed in [ArEhSo03] for the five-point finite difference scheme (of second order) for (1.1), along with the Crank-Nicolson time discretization. But the numerical tests of [ArEhSo03] were only for the 1D case. Here we shall follow the same strategy for a fourth order spatial discretization. Moreover we present 2D simulation results.

This article is organized as follows: In §2 we derive the compact fourth order scheme for the Schrödinger equation, and in §3 we construct the corresponding DTBCs, which are of convolution form. Their highly oscillatory convolution coefficients are analyzed and finally replaced by nicely decaying coefficients in §4. In the last section we present some numerical simulations to illustrate the effectiveness and accuracy of our DTBCs. Finally we give an application of inhomogeneous DTBCs to a 2D waveguide simulation with a T-shaped quantum transistor.

2 A fourth order difference scheme for the Schrödinger equation

In this section we consider the time-dependent Schrödinger equation on the whole space $\mathbb{R}^2$. Let $\Omega_{\Delta x,\Delta y}$ be an equidistant grid with the nodes $x_j = j\Delta x$, $y_k = k\Delta y$ for j, $k \in \mathbb{Z}$. In time we use the discretization $t_n = n\Delta t$, $n \in \mathbb{N}_0$, such that $\psi_{j,k}^n \sim \psi(x_j, y_k, t_n)$ denotes an approximation of the solution $\psi(x, y, t)$ of the Schrödinger equation (1.1). For the discretization of (1.1), we recall the standard finite difference operators

$$\begin{aligned} D_t^+ \psi_{j,k}^n &:= \frac{\psi_{j,k}^{n+1} - \psi_{j,k}^n}{\Delta t}, \\ D_x^2 \, \psi_{j,k}^n &:= \frac{\psi_{j-1,k}^n - 2\psi_{j,k}^n + \psi_{j+1,k}^n}{\Delta x^2}, \\ D_y^2 \, \psi_{j,k}^n &:= \frac{\psi_{j,k-1}^n - 2\psi_{j,k}^n + \psi_{j,k+1}^n}{\Delta y^2}, \end{aligned}$$

and the abbreviations

$$\begin{aligned} \psi_{j,k}^{n+\frac{1}{2}} &:= \frac{1}{2}\left(\psi_{j,k}^{n+1} + \psi_{j,k}^n\right), \\ V_{j,k}^{n+\frac{1}{2}} &:= V\left(x_j, y_k, t_{n+\frac{1}{2}}\right). \end{aligned}$$

Higher order finite difference schemes for the Schrödinger equation have been developed for example in [AvKoSi00], [KaMoSi05] and the references therein. Now we briefly recall

the derivation of compact, higher order schemes and prove their discrete L^2-conservation for the Schrödinger equation. Consider first the differential equation

$$\psi''(x) = f(x, \psi), \qquad x \in \mathbb{R}, \psi : \mathbb{R} \to \mathbb{C}. \tag{2.1}$$

The difference equation

$$D_x^2 \psi_j = \frac{1}{12}\big(f_{j+1} + 10 f_j + f_{j-1}\big), \qquad j \in \mathbb{Z} \tag{2.2}$$

yields a fourth order approximation of (2.1) (see [Co66]). In the physical literature this scheme is often called *Numerov's method*. Applying this scheme to the 1D time-dependent Schrödinger equation leads to the discretization

$$\begin{aligned} D_x^2\, \psi_j^{n+\frac{1}{2}} \;=\; & \frac{1}{6}\Big(V_{j-1}^{n+\frac{1}{2}} \psi_{j-1}^{n+\frac{1}{2}} - i D_t^+ \psi_{j-1}^n + 10 V_j^{n+\frac{1}{2}} \psi_j^{n+\frac{1}{2}} \\ & - 10 i D_t^+ \psi_j^n + V_{j+1}^{n+\frac{1}{2}} \psi_{j+1}^{n+\frac{1}{2}} - i D_t^+ \psi_{j+1}^n \Big) \end{aligned} \tag{2.3}$$

as described in [Mo04].

Consider now the two-dimensional Schrödinger equation. With the semidiscretization $\psi(x, y, t_n) \sim \psi^n(x, y)$ in time, the usual Crank-Nicolson scheme reads

$$\Delta \psi^{n+\frac{1}{2}}(x, y) = 2 V^{n+\frac{1}{2}}(x, y) \psi^{n+\frac{1}{2}}(x, y) - 2 i D_t^+ \psi^n(x, y). \tag{2.4}$$

In order to derive a higher order spatial discretization, the compact nine-point scheme (cf. [St04], e. g.) is applied to equation (2.4). With the finite difference operator

$$\widetilde{D}^2 := D_x^2 + D_y^2 + \frac{\Delta x^2 + \Delta y^2}{12} D_x^2\, D_y^2$$

and the identity operator I, this yields a new generalization of the 1D case from [Mo04]:

$$\widetilde{D}^2\, \psi_{j,k}^{n+\frac{1}{2}} = \left(I + \frac{\Delta x^2}{12} D_x^2 + \frac{\Delta y^2}{12} D_y^2\right) \Big[2 V_{j,k}^{n+\frac{1}{2}} \psi_{j,k}^{n+\frac{1}{2}} - 2 i D_t^+ \psi_{j,k}^n\Big]. \tag{2.5}$$

It approximates the solution of the Schrödinger equation (1.1) with the order $\mathcal{O}\left(\Delta x^4 + \Delta y^4 + \Delta t^2\right)$.

It is well known that the Schrödinger equation (in whole space or with homogeneous Dirichlet conditions) preserves the $L^2(\Omega)$-norm in time. Like the usual second order finite-difference Crank-Nicolson method, the fourth order scheme (2.5) preserves the discrete L^2-norm:

Lemma 2.1 (preservation of ℓ^2-norm) *Let the grid function $V^{n+\frac{1}{2}}$ be bounded for all $n \in \mathbb{N}_0$. For the whole space problems of the 1D and 2D time-dependent Schrödinger equation the schemes (2.3) and (2.5) then preserve the ℓ^2-norm in time.*

Proof: To unify the proof for both cases we define the following positive definite, bounded, and self-adjoint operators

$$A := I + \frac{\Delta x^2}{12} D_x^2 \qquad \text{on } \ell^2(\mathbb{Z})$$

and

$$A := I + \frac{\Delta x^2}{12} D_x^2 + \frac{\Delta y^2}{12} D_y^2 \qquad \text{on } \ell^2(\mathbb{Z}^2).$$

Also, we set $\widetilde{D}^2 := D_x^2$ for the 1D case (i.e. $d = 1$). Hence, (2.3) and (2.5) both have the form

$$\widetilde{D}^2 \psi^{n+\frac{1}{2}} = A \left[2V^{n+\frac{1}{2}} \psi^{n+\frac{1}{2}} - 2iD_t^+ \psi^n \right],$$

or

$$iD_t^+ \psi^n \;=\; V^{n+\frac{1}{2}} \psi^{n+\frac{1}{2}} - \frac{1}{2} A^{-1} \widetilde{D}^2 \psi^{n+\frac{1}{2}}, \tag{2.6}$$

since A is invertible.

It remains to show that the r.h.s. of (2.6) is self-adjoint on $\ell^2(\mathbb{Z}^d)$, as this implies the preservation of the ℓ^2-norm. Defining the operator $B := I - A$ yields $||B|| \leq \frac{2}{3}$. Hence, $\sum_{n=0}^{\infty} B^n = (I - B)^{-1} = A^{-1}$. Since B commutes with $\widetilde{D}$, also A^{-1} does. Hence, $V^{n+\frac{1}{2}} - \frac{1}{2} A^{-1} \widetilde{D}^2$ is self-adjoint and the assertion follows.

□

3 Discrete transparent boundary conditions for the fourth order difference scheme

As in §1, we consider here the Schrödinger equation

$$\begin{aligned} i\frac{\partial}{\partial t}\psi(x,y,t) &= -\frac{1}{2}\Delta\psi(x,y,t) + V(x,y,t)\psi(x,y,t), \quad t > 0 \\ \psi(x,y,0) &= \psi^I(x,y), \qquad (x,y) \in \Omega \\ \psi(x,0,t) &= \psi(x,Y,t) = 0, \qquad x \in \mathbb{R},\, t > 0, \end{aligned} \tag{3.1}$$

on the infinite stripe $\Omega = \mathbb{R} \times (0, Y)$ with some $Y > 0$. We assume that the initial function $\psi^I \in L^2(\Omega)$ has compact support

$$supp\ \psi^I(x,y) \subset (0,X) \times (0,Y) =: \Omega_{comp}, \tag{3.2}$$

which will be our computational domain. The potential $V(x,y,t)$ is assumed to be an $L^\infty(\Omega_{comp} \times \mathbb{R}^+)$ function in space and time, and constant on each of the two exterior

domains.

In this section we shall derive at $x = 0$ and $x = X$ discrete transparent boundary conditions for (3.1), discretized by the scheme (2.5). With the equidistant grid $\Omega_{\Delta x,\Delta y} = (j\Delta x, k\Delta y)$ for $j \in \mathbb{Z}$; $k = 0, \ldots, K \in \mathbb{N}$; $t_n = n\Delta t$, $n \in \mathbb{N}_0$ and the abbreviations

$$\begin{aligned} D &:= \frac{\Delta x^2}{\Delta y^2}, \\ C &:= \frac{\Delta x^2 + \Delta y^2}{12\Delta y^2}, \\ W &:= \frac{i\Delta x^2}{3\Delta t}, \\ \alpha_{j,k}^n &:= 2C - W + \frac{\Delta x^2}{6} V_{j,k}^{n+\frac{1}{2}}, \\ \beta_{j,k}^n &:= -2 - 2D - 8\alpha_{j,k}^n + 20C \end{aligned}$$

the discretization of (3.1) with scheme (2.5) reads explicitly:

$$\begin{aligned} &(1 - \alpha_{j+1,k}^n)\, \psi_{j+1,k}^{n+1} + (1 - \alpha_{j-1,k}^n)\, \psi_{j-1,k}^{n+1} + (D - \alpha_{j,k+1}^n)\psi_{j,k+1}^{n+1} + (D - \alpha_{j,k-1}^n)\psi_{j,k-1}^{n+1} \\ &+ \beta_{j,k}^n\, \psi_{j,k}^{n+1} + C\left[\psi_{j-1,k-1}^{n+1} + \psi_{j-1,k+1}^{n+1} + \psi_{j+1,k-1}^{n+1} + \psi_{j+1,k+1}^{n+1}\right] \\ &= (2W - 1 + \alpha_{j+1,k}^n)\psi_{j+1,k}^n + (2W - 1 + \alpha_{j-1,k}^n)\psi_{j-1,k}^n \\ &\quad + (2W - D + \alpha_{j,k+1}^n)\psi_{j,k+1}^n + (2W - D + \alpha_{j,k-1}^n)\psi_{j,k-1}^n + (16W - \beta_{j,k}^n)\psi_{j,k}^n \\ &\quad - C\left[\psi_{j-1,k-1}^n + \psi_{j-1,k+1}^n + \psi_{j+1,k-1}^n + \psi_{j+1,k+1}^n\right]; \quad j \in \mathbb{Z};\, k = 1, \ldots, K;\, n \in \mathbb{N}_0. \end{aligned} \tag{3.3}$$

The idea of deriving DTBCs is to eliminate the exterior problem by using the explicit solution on the outer domain $\Omega \setminus \Omega_{comp}$. This is the reason for assuming a uniform grid on Ω_{comp}^C. On Ω_{comp}, however, the grid can be non-uniform, or even adaptive in time. Following the strategy of [ArEhSo03], this is done with a $\mathfrak{Z}$-transformation in time and a discrete sine-transformation in y-direction. The outer grid domain $\Omega_{\Delta x,\Delta y}^C = (j\Delta x, k\Delta y)$ for $j \le 0$, $j \ge J$, $0 \le k \le K$, $j, k \in \mathbb{Z}$ is divided into $K - 1$ stripes. Hence, we get $K - 1$ linearly independent modes, because the potential is assumed to be constant on $\Omega_{\Delta x,\Delta y}^C$. The DTBCs in [ArEhSo03] were obtained for the Schrödinger equation discretized with a second order difference scheme. Recently in [Mo04] and [Mo06] the author adapted the DTBCs from [ArEhSo03] for the 1D Schrödinger equation discretized with the higher order scheme (2.3) – in [Mo04] for the time-dependent and in [Mo06] for the steady-state case.

With the discrete sine-transform in y-direction on $\Omega^C_{\Delta x,\Delta y}$

$$\widehat{\psi}^n_{j,m} := \frac{2}{K}\sum_{k=1}^{K-1} \psi^n_{j,k} \sin\left(\frac{\pi k\, m}{K}\right), \qquad m = 1,\ldots,K-1, \tag{3.4}$$

a new system for the modes $\widehat{\psi}^n_{j,m}$, $m = 1,\ldots,K-1$, $j \le 0$ and $j \ge J$ follows:

$$\begin{aligned}\gamma_m\, \widehat{\psi}^{n+1}_{j+1,m} \;+\; \gamma_m\, \widehat{\psi}^{n+1}_{j-1,m} + \rho_m\, \widehat{\psi}^{n+1}_{j,m} \\ = (2W-\gamma_m)\, \widehat{\psi}^n_{j+1,m} + (2W-\gamma_m)\, \widehat{\psi}^n_{j-1,m} + (\kappa_m-\rho_m)\, \widehat{\psi}^n_{j,m},\end{aligned} \tag{3.5}$$

with the abbreviations

$$\begin{aligned}\gamma_m &:= 1 + 2C\left(\cos\left(\frac{\pi m}{K}\right) - 1\right) + W - \frac{\Delta x^2}{6}V,\\ \kappa_m &:= 4\left(\cos\left(\frac{\pi m}{K}\right) + 4\right) W,\\ \rho_m &:= -2 - 2D + 4C + 8W - \frac{4\Delta x^2}{3}V\\ &\quad + \left(2D - 4C + 2W - \frac{\Delta x^2}{3}V\right)\cos\left(\frac{\pi m}{K}\right), \qquad m = 1,\ldots,K-1.\end{aligned} \tag{3.6}$$

While the potential may take different constant values on each semiinfinite, exterior stripe, we skipped this dependence in the above constants to simplify the notation. Next we $\mathfrak{Z}$-transform the system (3.5) using

$$\mathfrak{Z}\left(\widehat{\psi}^n_{j,m}\right) := \Phi_{j,m}(z) := \sum_{n=0}^{\infty} \widehat{\psi}^n_{j,m} z^{-n} \qquad \text{with } z \in \mathbb{C},\ |z| > 1.$$

We shall discuss here the derivation of the DTBCs at the right boundary, i.e. $j = J$; the case $j = 0$ is completely analogous. We choose the initial function $\psi^0_{j,k}$ such that $\psi^0_{j,k} = 0$ for all $j \ge J-1$, $j \le 1$ and all k. Hence

$$\widehat{\psi}^0_{J+1,m} = \widehat{\psi}^0_{J-1,m} = \widehat{\psi}^0_{J,m} = 0, \quad m = 1,\ldots,K-1.$$

The $\mathfrak{Z}$-transformed system (3.5) reads

$$\begin{aligned}\Phi_{j+1,m}(z) + \left[\frac{\rho_m(z+1)-\kappa_m}{\gamma_m(z+1)-2W}\right]\Phi_{j,m}(z) + \Phi_{j-1,m}(z) &= 0,\\ j \ge J,\ m = 1,\ldots,K-1.\end{aligned} \tag{3.7}$$

This is a this second order finite difference equation (in the j-variable). Its characteristic equation has two solutions $\nu^{(1)}_m(z)$, $\nu^{(2)}_m(z)$. For each mode $m = 1,\ldots,K-1$ we shall only

consider the one solution satisfying $|\nu_m(z)| < 1$. The corresponding, decaying solution $\Phi_{j,m}(z) = (\nu_m(z))^j$, $j \geq J$ of (3.7) then yields the $\mathfrak{Z}$-transformed DTBCs at $j = J$ for each mode:

$$\Phi_{J,m}(z) = \nu_m(z)\Phi_{J-1,m}(z)$$

with

$$\nu_{J,m}(z) \;=\; \frac{-\rho_{J,m}(z+1) + \kappa_m + \sqrt{\zeta_{J,m}z^2 - 2\xi_{J,m}z + \theta_{J,m}}}{2\gamma_{J,m}(z - \eta_{J,m})}. \tag{3.8}$$

Here, we use the constants

$$\begin{aligned}
\eta_{J,m} &:= \frac{2W}{\gamma_{J,m}} - 1, \\
\zeta_{J,m} &:= (\rho_{J,m})^2 - 4(\gamma_{J,m})^2, \\
\theta_{J,m} &:= (\kappa_m - \rho_{J,m})^2 - 4(\gamma_{J,m}\eta_{J,m})^2, \\
\xi_{J,m} &:= -(\rho_{J,m})^2 - 4(\gamma_{J,m})^2\eta_{J,m} + \rho_{J,m}\kappa_m,
\end{aligned} \tag{3.9}$$

for $m = 1, \ldots, K-1$ and analogously for $j \leq 0$. With some work one can calculate analytically the $\mathfrak{Z}$-inverse of (3.8): $\mathfrak{Z}^{-1}(\nu_{J,m}(z))^{(n)} =: \ell_{J,m}^{(n)}$, which leads to the following theorem:

Theorem 3.1 (DTBCs for the 2D Schrödinger equation) *The sine-transformed DTBCs at $j = 0$ and $j = J$ for the discretization scheme (3.3) read*

$$\widehat{\psi}_{1,m}^n - \ell_{0,m}^{(0)}\widehat{\psi}_{0,m}^n \;=\; \sum_{k=1}^{n-1} \ell_{0,m}^{(n-k)}\widehat{\psi}_{0,m}^k, \qquad n \geq 1, \tag{3.10}$$

$$\widehat{\psi}_{J-1,m}^n - \ell_{J,m}^{(0)}\widehat{\psi}_{J,m}^n \;=\; \sum_{k=1}^{n-1} \ell_{J,m}^{(n-k)}\widehat{\psi}_{J,m}^k, \qquad n \geq 1. \tag{3.11}$$

The coefficients $\ell_{j,m}^{(n)}$ for $j = 0, J$, $m = 1, \ldots, K-1$ and $n \geq 0$ are given by

$$\begin{aligned}
\ell_{j,m}^{(n)} \;=\; & -\frac{\rho_{j,m}}{2\gamma_{j,m}}\eta_{j,m}^n + \frac{\kappa_m - \rho_{j,m}}{2\gamma_{j,m}}\left(\eta_{j,m}^{n-1} - \frac{1}{\eta_{j,m}}\delta_n^0\right) \\
& + \frac{\sqrt{\theta_{j,m}}}{2\gamma_{j,m}}\lambda_{j,m}^{1-n}\left[P_n(\mu_{j,m}) - \frac{P_{n-1}(\mu_{j,m})}{\eta_{j,m}\lambda_{j,m}} + \frac{\tau_{j,m}}{\zeta_{j,m}\eta_{j,m}}\sum_{k=0}^{n-1}(\lambda_{j,m}\eta_{j,m})^{n-k}P_k(\mu_{j,m})\right],
\end{aligned} \tag{3.12}$$

with the Legendre polynomials P_n ($P_{-1} \equiv 0$), the Kronecker symbol δ_n^0, and the abbreviations used in (3.6), (3.9) and

$$\begin{aligned}
\lambda_{j,m} &:= \frac{\sqrt{\zeta_{j,m}}}{\sqrt{\theta_{j,m}}}, \\
\mu_{j,m} &:= \frac{\xi_{j,m}}{\sqrt{\theta_{j,m}}\sqrt{\zeta_{j,m}}}, \\
\tau_{j,m} &:= \frac{\theta_{j,m}}{\eta_{j,m}} + \zeta_{j,m}\eta_{j,m} - 2\xi_{j,m}.
\end{aligned}$$

For all j, m holds $\theta_{j,m} = \bar{\zeta}_{j,m}$, thus one can verify $|\lambda_{j,m}| = 1$.

Remark 3.2 *In (3.10), (3.11) the DTBCs are written in the sine-transformed space. Since they are local in the y-Fourier space, this is the efficient way to implement them. A direct implementation in position space would necessitate much bigger numerical costs. Thus the discrete convolution*

$$\hat{C}_{J,m}^{(n-1)} := \frac{1}{K} \sum_{\nu=1}^{n-1} \ell_{J,m}^{(n-\nu)} \hat{\psi}_{J,m}^{\nu}, \quad m = 1, \ldots, K-1$$

for the right boundary at $x_J = J\Delta x$ is calculated in Fourier space and inverse transformed.The left hand sides of (3.10), (3.11) have to be transformed back also into position space. Hence, we get a coupling between all boundary points.

4 Asymptotic behaviour of the convolution coefficients

Just like for the one-dimensional case [EhAr01] and for the standard five-point finite difference scheme for the two-dimensional Schrödinger equation [ArEhSo03], the convolution coefficients (3.12) are highly oscillatory as a function of $n \in \mathbb{N}_0$. Figure 1(a) shows the real part of the convolution coefficients $\ell_{J,m}^{(n)}$ of the DTBCs for the Schrödinger equation calculated on the domain $\Omega = (0,1) \times (0,1)$ with the parameters $\Delta x = \Delta y = 0.02$, $\Delta t = 2 \cdot 10^{-5}$, $V = 0$ as a function of the time steps $n = 0, \ldots, 1000$.

Lemma 4.1 *For large n, the convolution coefficients $\ell_{j,m}^{(n)}$ given in (3.12) have the asymptotic behaviour*

$$\ell_{j,m}^{(n)} \sim \sigma_{j,m}\, e^{i\vartheta_{j,m} n} \tag{4.1}$$

as $n \to \infty$, with

$$\sigma_{j,m} := -\frac{\rho_{j,m}}{2\gamma_{j,m}} + \frac{\kappa_m - \rho_{j,m}}{2\gamma_{j,m}\eta_{j,m}} + \frac{\sqrt{\tau_{j,m}}}{2\gamma_{j,m}\sqrt{\eta_{j,m}}}, \quad \vartheta_{j,m} = \arg(\eta_{j,m})$$

for $j = 0$, J and $m = 1, \ldots, K-1$.

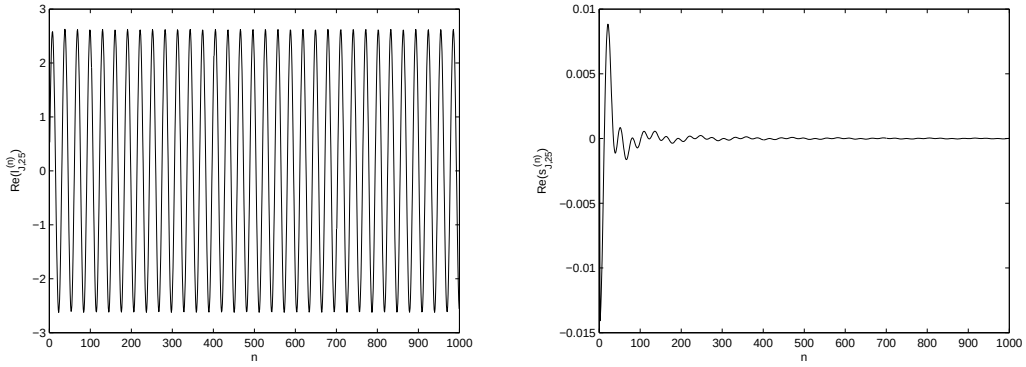

(a) original coefficients $\ell^{(n)}$ (b) summed coefficients $s^{(n)}$

Figure 1: Time dependence of the convolution coefficients. For both plots we have taken $\Delta x = \Delta y = 0.02$, $V = 0$, and $\Delta t = 2 \cdot 10^{-5}$. Figure 1(a) shows the real part of the convolution coefficients $\ell_{J,m}^{(n)}$ for the mode $m = 25$ as a function of the time step $n = 0, \ldots, 1000$. The real part of modified convolution coefficients $s_{J,m}^{(n)} := \ell_{J,m}^{(n)} - \eta_{J,m}\ell_{J,m}^{(n-1)}$ for $n \geq 2$ is plotted in Figure 1(b).

Proof: For all $j = 0, J$; $m = 1, \ldots, K-1$ it holds $|\eta_{j,m}| = |\lambda_{j,m}| = 1$ and $\mu_{j,m} \in \mathbb{R}$. Additionally one can verify (with Maple, e.g.) that $|\mu_{j,m}| < 1$ for all $j = 0, J$; $m = 1, \ldots, K-1$. Hence, there exists the representation

$$\begin{aligned} \lambda_{j,m} &= e^{i\varphi_{j,m}}, & \varphi_{j,m} \in \mathbb{R}, \\ \eta_{j,m} &= e^{i\vartheta_{j,m}}, & \vartheta_{j,m} \in \mathbb{R}, \\ \mu_{j,m} &= \cos(\omega_{j,m}), & 0 < \omega_{j,m} < \pi. \end{aligned}$$

With the formula of Laplace (cf. [Sz75]) follows

$$P_n(\cos(\omega_{j,m})) = \frac{\sqrt{2}}{\sqrt{\pi \sin(\omega_{j,m})}} \frac{\cos\left[\left(n + \frac{1}{2}\right)\omega_{j,m} - \frac{\pi}{4}\right]}{\sqrt{n}} + \mathcal{O}(n^{-3/2}), \tag{4.2}$$

where the bound of the error term holds uniformly in the interval $\epsilon \leq \omega_{j,m} \leq \pi - \epsilon$ for all $\epsilon > 0$. Hence we have

$$\lim_{n\to\infty} P_n(\cos(\omega_{j,m})) = 0$$

uniformly on $\epsilon \leq \omega_{j,m} \leq \pi - \epsilon$ for any $\epsilon > 0$. From (3.12) then follows

$$\begin{aligned} \ell_{j,m}^{(n)} &= -\frac{\rho_{j,m}}{2\gamma_{j,m}} e^{i\vartheta_{j,m}n} + \frac{\kappa_{j,m} - \rho_{j,m}}{2\gamma_{j,m}} e^{i\vartheta_{j,m}(n-1)} \\ &\quad + \frac{\sqrt{\theta_{j,m}}\tau_{j,m}}{2\gamma_{j,m}\zeta_{j,m}} e^{i\vartheta_{j,m}(n-1)} e^{i\varphi_{j,m}} \sum_{k=0}^{n-1} e^{-i(\varphi_{j,m}+\vartheta_{j,m})k} P_k(\mu_{j,m}) + \mathcal{O}\left(\frac{1}{\sqrt{n}}\right) \end{aligned}$$

for n large. For $|2r\mu - r^2| < 1$ it holds

$$\sum_{k=0}^{\infty} r^k P_k(\mu) = \frac{1}{\sqrt{1-2r\mu+r^2}}$$

(cf. [Do51]). One can verify (again with Maple, e.g.) that $\left|\frac{2\mu_{j,m}}{\eta_{j,m}\lambda_{j,m}} - \frac{1}{(\eta_{j,m}\lambda_{j,m})^2}\right| < 1$ for all $j = 0, J$; $m = 1, \ldots, K-1$. This yields

$$\lim_{n\to\infty} \sum_{k=0}^{n-1} e^{-i(\varphi_{j,m}+\vartheta_{j,m})k} P_k(\mu_{j,m}) \quad = \quad \sqrt{\frac{\zeta_{j,m}\eta_{j,m}}{\tau_{j,m}}},$$

and finally

$$\lim_{n\to\infty} e^{-i\vartheta_{j,m}n} \ell_{j,m}^{(n)} \quad = \quad -\frac{\rho_{j,m}}{2\gamma_{j,m}} + \frac{\kappa_{j,m}-\rho_{j,m}}{2\gamma_{j,m}\eta_{j,m}} + \frac{\sqrt{\tau_{j,m}}}{2\gamma_{j,m}\sqrt{\eta_{j,m}}}.$$

□

Lemma 4.1 shows, that the convolution coefficients $\ell_{j,m}^{(n)}$ are asymptotically an oscillatory sequence. Moreover, this behaviour deviates from the $\mathcal{O}(t^{-3/2})$-decay of the continuous convolution kernel in (1.3). Hence, it may lead to numerical cancellations in the calculation of the convolution sums (3.10), (3.11). As an alternative we shall derive coefficients that decay like $\mathcal{O}(n^{-3/2})$. For the left DTBCs we therefore add equation (3.10) for n and $n-1$ with the corresponding weighting factors 1 and $-e^{i\vartheta_{1,m}} = -\eta_{1,m}$ (the case $j = J$ is analogous) and proceed like in [EhAr01]. This gives the following reformulated DTBCs

$$\widehat{\psi}_{1,m}^{n} - s_{0,m}^{(0)} \widehat{\psi}_{0,m}^{n} \quad = \quad \sum_{k=1}^{n-1} s_{0,m}^{(n-k)} \widehat{\psi}_{0m}^{k} + \eta_{1,m} \widehat{\psi}_{1,m}^{n-1}, \tag{4.3}$$

$$\widehat{\psi}_{J-1,m}^{n} - s_{J,m}^{(0)} \widehat{\psi}_{J,m}^{n} \quad = \quad \sum_{k=1}^{n-1} s_{J,m}^{(n-k)} \widehat{\psi}_{Jm}^{k} + \eta_{J-1,m} \widehat{\psi}_{J-1,m}^{n-1}, \tag{4.4}$$

for $n \geq 1$ with the *summed coefficients*

$$s_{j,m}^{(n)} := \begin{cases} \ell_{j,m}^{(n)} - \eta_{j,m}\, \ell_{j,m}^{(n-1)}, & n \geq 1, \\ \ell_{j,m}^{(0)}, & n = 0, \end{cases} \tag{4.5}$$

for $m = 1, \ldots, K-1$; $j = 0$ and $j = J$.

Lemma 4.2 *For $n \geq 2$, the summed coefficients (4.5) can be calculated by the formula*

$$s_{j,m}^{(n)} \quad = \quad -\frac{\sqrt{\theta_{j,m}}}{2\gamma_{j,m}} \lambda_{j,m}^{1-n} \frac{P_n(\mu_{j,m}) - P_{n-2}(\mu_{j,m})}{2n-1}$$

or by the recursion

$$s_{j,m}^{(n+1)} = \frac{2n-1}{n+1}\frac{\mu_{j,m}}{\lambda_{j,m}} s_{j,m}^{(n)} - \frac{n-2}{n+1}(\lambda_{j,m})^{-2} s_{j,m}^{(n-1)} \tag{4.6}$$

for $j = 0,\ J$ *and* $m = 1, \ldots, K-1$. *These new coefficients have the asymptotic behaviour*

$$s_{j,m}^{(n)} \ \sim \mathcal{O}(n^{-3/2}). \tag{4.7}$$

Proof: Using (3.12), the summed coefficients read for $n \geq 2$

$$\begin{aligned} s_{j,m}^{(n)} \ &= \ \frac{\sqrt{\theta_{j,m}}}{2\gamma_{j,m}} \lambda_{j,m}^{1-n} \Big[P_n(\mu_{j,m}) + P_{n-2}(\mu_{j,m}) - \frac{1}{\lambda_{j,m}\eta_{j,m}} P_{n-1}(\mu_{j,m}) \\ &\quad - \eta_{j,m}\lambda_{j,m} P_{n-1}(\mu_{j,m}) + \frac{\tau_{j,m}\lambda_{j,m}}{\zeta_{j,m}} P_{n-1}(\mu_{j,m}) \Big]. \end{aligned}$$

And with the recursion for the Legendre polynomials,

$$\frac{n}{2n-1} P_n(\mu_{j,m}) + \frac{n-1}{2n-1} P_{n-2}(\mu_{j,m}) \ = \ \mu_{j,m} P_{n-1}(\mu_{j,m}), \tag{4.8}$$

for $n \geq 2$ then follows

$$s_{j,m}^{(n)} \ = \ -\frac{\sqrt{\theta_{j,m}}}{2\gamma_{j,m}} \lambda_{j,m}^{1-n} \frac{P_n(\mu_{j,m}) - P_{n-2}(\mu_{j,m})}{2n-1}. \tag{4.9}$$

This representation of the convolution coefficients is analogous to the DTBCs for the one dimensional Schrödinger equation [EhAr01] and for the five-point stencil in the two dimensional case [ArEhSo03]. Hence, the recurrence formula of §3.3 in [EhAr01] applies also here, and it gives (4.6). For the same reason, also the asymptotic behaviour $s_{j,m}^{(n)} \sim \mathcal{O}(n^{-3/2})$ carries over from [EhAr01]. There, it is derived by applying equation (4.2) to the Legendre recursion (4.8) for $P_n(\mu_{j,m}) - P_{n-2}(\mu_{j,m})$.

□

Remark 4.3 *The decay rate (4.7) of the summed convolution coefficients coincides with the decay* $\mathcal{O}(t^{-3/2})$ *of the convolution kernel in the analytical TBC in (1.3) (cf. Fig 2). Figure 1(b) shows the real part of the summed coefficients (4.5) corresponding to the ones presented in Figure 1(a).*

Remark 4.4 *Like the analytical TBC (1.2), the DTBCs (4.3), (4.4) are non-local in time. For the calculation of the solution* $\psi_{j,m}^n$ *of the discretized Schrödinger equation (2.5), it is necessary to compute a convolution of size n in the n-th time step, which leads to a quadratically growing numerical effort. In [ArEhSo03] the authors derived an approximation of the convolution coefficients by a sum-of-exponentials. Since we have*

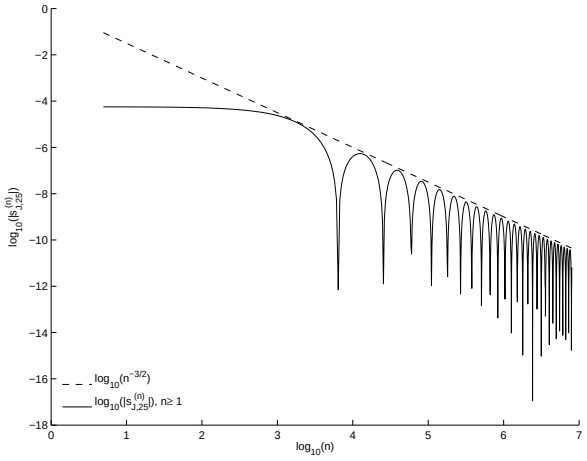

Figure 2: Algebraic decay rate of the new summed coefficients. The figure presents $\left|s_{J,m}^{(n)}\right|$ as a function of the time step $n = 1, \ldots, 1000$. $\left|s_{J,25}^{(n)}\right|$ is plotted for $\Delta t = 2{\cdot}10^{-5}$, $\Delta x = \Delta y = 0.02$ and $V = 0$ (solid line) and compared to $\log_{10}(n^{-3/2})$ (dashed line).

the same recursion formulas for the summed convolution coefficients (4.5) for the higher order difference scheme like the coefficients in [ArEhSo03] for the second order scheme, we can use their results on the approximation of the convolution coefficients. It is shown there, that the convolution coefficients can be approximated very efficiently by the sum of exponentials. With this approach, the numerical costs of the discrete convolutions in our DTBCs can be reduced from $\mathcal{O}(KN^2)$ to $\mathcal{O}(KLN)$, where K denotes the number of modes, N the total number of time steps, and L the number of exponential terms in the approximation. Typical values to obtain good results are $L =$ 10-20. This is a very important result for long-time simulations or even the calculation of steady-states via a time-stepping approach.

5 Numerical tests

In this section we present some numerical results and applications of DTBCs in two dimensions. First, we verify numerically the accuracy of the DTBCs for the free Schrödinger equation. Then we apply DTBCs to the simulation of the electron transport through a quantum waveguide.

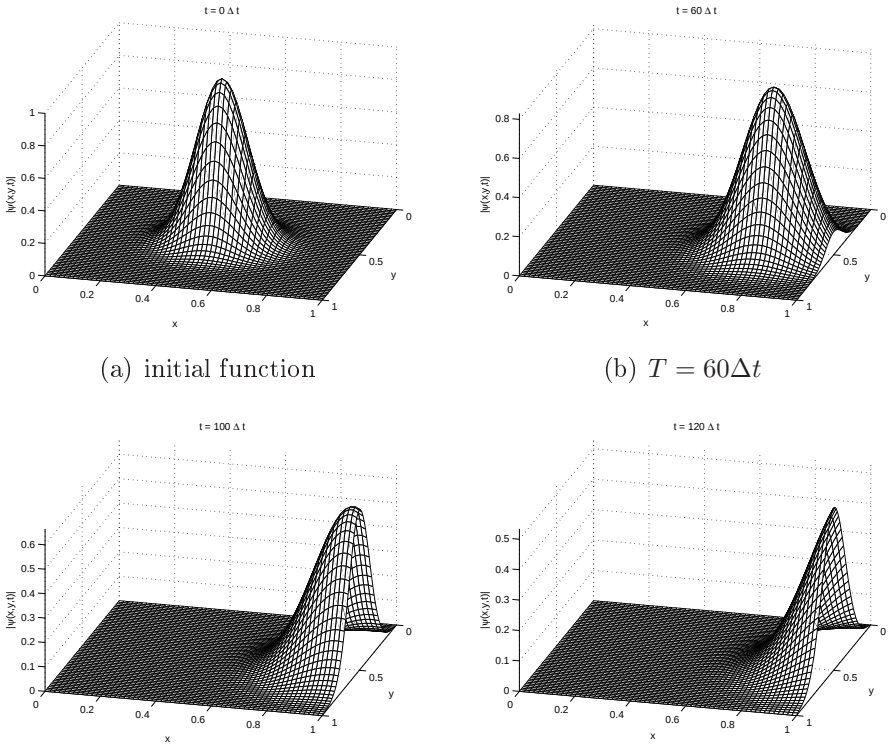

(a) initial function

(b) $T = 60\Delta t$

(c) $T = 100\Delta t$

(d) $T = 120\Delta t$

Figure 3: Orthogonal incidence at the boundary: absolute value of the calculated solution to the time-dependent Schrödinger equation with the initial function (5.1) on the computational domain $(0,1) \times (0,1)$ with $\Delta x = \Delta y = 1/120$, $\Delta t = 2 \cdot 10^{-4}$, and the wavenumber $k_x = 50$. The potential equals 0; DTBCs are implemented at $x = 0$ and $x = 1$.

5.1 Travelling Gaussian wave functions

In the first example we study the time evolution of a Gaussian wave in a two-dimensional channel $\Omega = \mathbb{R} \times (0,1)$. Since the analytical solution is known here, this is a good example to test the DTBCs.

To get homogeneous Dirichlet boundary conditions at the channel walls $y = 0$ and $y = 1$, we consider the y-periodic initial function

$$\psi^I(x,y) = \sum_{l \in \mathbb{Z}} (-1)^l e^{-\frac{\alpha}{2}\left[\left(x-\frac{1}{2}\right)^2 + \left(y-\frac{1}{2}+l\right)^2\right] - ik_x\left(x-\frac{1}{2}\right)} \tag{5.1}$$

on the domain Ω with some $\alpha > 0$. Using the computational domain $\Omega_{comp} = (0,1)^2$ we consider DTBCs at $x = 0$ and $x = 1$. The wave will travel along the channel in

x-direction with the velocity given by the wavenumber $k_x > 0$ and it will cross the transparent boundary at $x = 1$ without any reflections. The solution of the time-dependent Schrödinger equation with the initial function (5.1) can be expressed analytically by

$$\psi_{ex}(x,y,t) = \frac{1}{1+i\alpha t}\sum_{l\in\mathbb{Z}}(-1)^l e^{\frac{-1}{2+2i\alpha t}\left(\alpha\left[\left(x-\frac{1}{2}\right)^2+\left(y-\frac{1}{2}+l\right)^2\right]-2ik_x\left(x-\frac{1}{2}\right)+ik_x^2 t\right)}, \quad t>0,$$

such that it is possible to compare the calculated solution ψ with the exact solution ψ_{ex}. Figure 3 shows the absolute value of the calculated solution $\psi(x,y,t)$ at some times t_n with the discretization parameters $\Delta x = \Delta y = 1/120$, $\Delta t = 2\cdot 10^{-4}$, $\alpha = 120$, and the wavenumber $k_x = 50$. The wave leaves Ω_{comp} without reflections. For these discretization parameters we compare in Figure 4(a) the relative error

$$L_1(t) = \frac{||\psi(.,.,t) - \psi_{ex}(.,.,t)||_{\ell^2(\Omega_{\Delta x,\Delta y})}}{||\psi^I(.,.)||_{\ell^2(\Omega_{\Delta x,\Delta y})}} \tag{5.2}$$

of the standard five-point scheme with the nine-point scheme. As expected the higher order scheme has a much smaller error. We remark that the wave packet has essentially crossed the artificial boundary at $T = 200\Delta t$.

In order to satisfy the assumption that ψ^I is compactly supported in Ω_{comp} (cf. §3) we used a small cut-off close to $x = 0$ and $x = 1$. This amounted to a relative ℓ^2-error on $\mathbb{R}\times(0,1)$ of $\mathcal{O}(10^{-8})$.

Next we compare the calculated solution ψ on $(0,1)\times(0,1)$ with a (more exact) reference solution ψ_2 calculated on $(0,2)\times(0,1)$ using DTBCs at $x = 0$ and $x = 2$ in order to distinguish between the error due to the difference scheme and to the DTBCs. Figure 4(b) shows the relative error

$$L_2(t) = \frac{||\psi(.,.,t) - \psi_2(.,.,t)||_{\ell^2(\Omega_{\Delta x,\Delta y})}}{||\psi^I(.,.)||_{\ell^2(\Omega_{\Delta x,\Delta y})}} \tag{5.3}$$

as a logarithmic plot for the same discretization parameters as before. Both ψ and ψ_2 were calculated with the compact nine-point difference scheme. With $L_2 \in \mathcal{O}(10^{-9})$, the error due to the DTBCs is much smaller than the error L_1 of the interior PDE-scheme.

The first example has shown a Gaussian wave travelling only in x-direction and hitting the artificial boundary orthogonally. Now we modify this example and consider the initial function

$$\psi^I(x,y) = \sum_{l\in\mathbb{Z}} e^{-120\left[\left(x-\frac{1}{4}\right)^2+\left(y-\frac{1}{4}+l\right)^2\right]-ik_x x-ik_y y}, \quad k_x,\, k_y \in \mathbb{R} \tag{5.4}$$

on the same computational domain $\Omega = (0,1)\times(0,1)$. As shown in Figure 5, the wave packet passes the boundary $x = 1$ in a non-orthogonal angle (45° here) without any

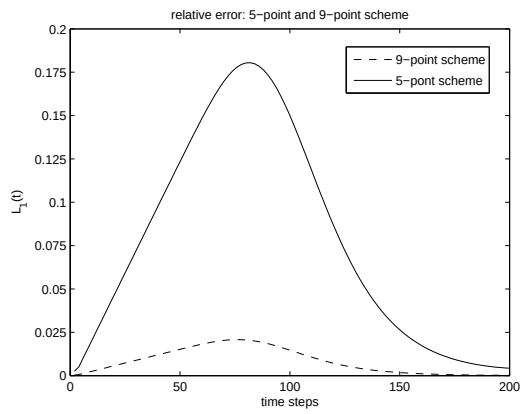

(a) Relative error L_1

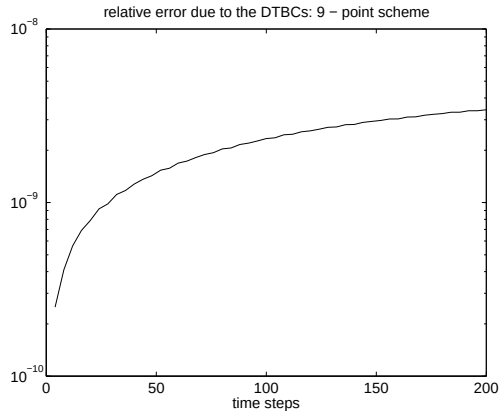

(b) Relative error L_2

Figure 4: Relative ℓ^2–errors of a travelling wave solution with the initial value (5.1) as a function of the time steps $n = 0, \ldots, 200$. (a): relative error L_1 of the finite difference scheme for the standard five-point scheme (solid line) and for the nine-point scheme (dashed line). (b): relative error L_2 of the DTBCs for the nine-point scheme. In all cases we used the parameters $\Delta x = \Delta y = 1/120$, $\Delta t = 2 \cdot 10^{-4}, \alpha = 120$, $k_x = 50$.

reflections. This example illustrates the *angular independence* of our DTBCs. In contrast to this situation here, local TBCs as introduced for wave-type equations in [EnMa77] and ABCs calculated with the potential ansatz [Bu97] show a strong dependence on the impact angle at the artificial boundary.

5.2 Simulation of quantum waveguides

Next we turn to a physical application of DTBCs. Open boundary conditions are a crucial ingredient for Schrödinger based simulations of the electron transport through quantum semiconductor devices. Typical examples include the ballistic transport along the channel of MOSFETs (cf. [JiLu02], [WaPoLu04]) or quantum waveguides (cf. [Bu97] or §13.4 of [Ra02] for an analysis of T-shaped *quantum interference transistors*). These are novel electronic switches of nano-scale dimensions. They are made of several different layers of semiconductor materials such that the electron flow is confined to small channels or waveguides. Due to their sandwiched structure the relevant geometry for the electron current is essentially two dimensional. Following the simulation of a GaAs-waveguide in [Bu97], we choose the T-shaped *quantum interference transistor* shown in Figure 6. The actual structure can be realized as an etched layer of GaAs between two layers of doped AlGaAs. Applying an external potential at the gate (i.e. above the shaded portion of the stub, the "allowed region" for the electrons, and

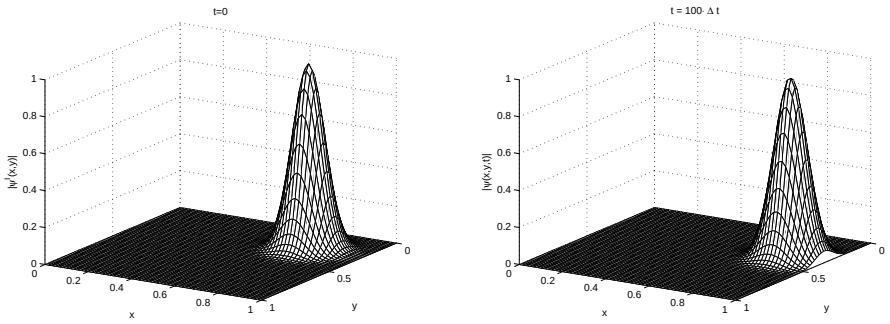

(a) initial function (b) $T = 100\Delta t$

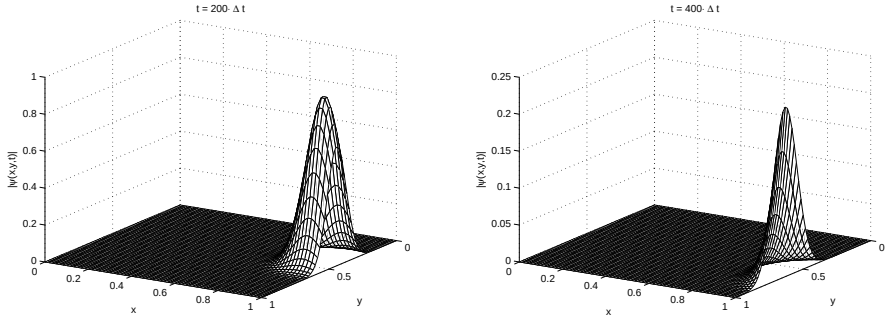

(c) $T = 200\Delta t$ (d) $T = 400\Delta t$

Figure 5: Non-orthogonal incidence at the boundary: absolute value of the calculated solution of the time-dependent Schrödinger equation with the initial function (5.4) on the computational domain $(0,1)\times(0,1)$ with $\Delta x = \Delta y = 1/120$, $\Delta t = 2 \cdot 10^{-5}$ and the wavevector $k = (100, -100)$. The potential equals 0; DTBCs are implemented at $x = 0$ and $x = 1$.

hence the geometry (in particular the stub length) can be modified (cf. [AiYaMi93], [ASSHFLL96] for experimental realizations). This allows to control the current flow through such an electronic device. It makes it a switch, which resambles a transistor – but on a nano-scale. With respect to small changes in the applied potential and the geometry, such a device shows sharp peaks in conductance that are due to the presence of bound states in the stub. It is expected that these novel devices will operate at low power and high speed.

The electron flow in these devices is modeled by the 2D Schrödinger equation

$$i\hbar\frac{\partial}{\partial t}\psi \;=\; -\frac{\hbar^2}{2m_*}\Delta\psi + V(x,y,t)\psi, \quad (x,y)\in\Omega,\, t>0\,, \tag{5.5}$$

with the Planck constant $\hbar$. And m_* is the effective mass of electrons in the semicon-

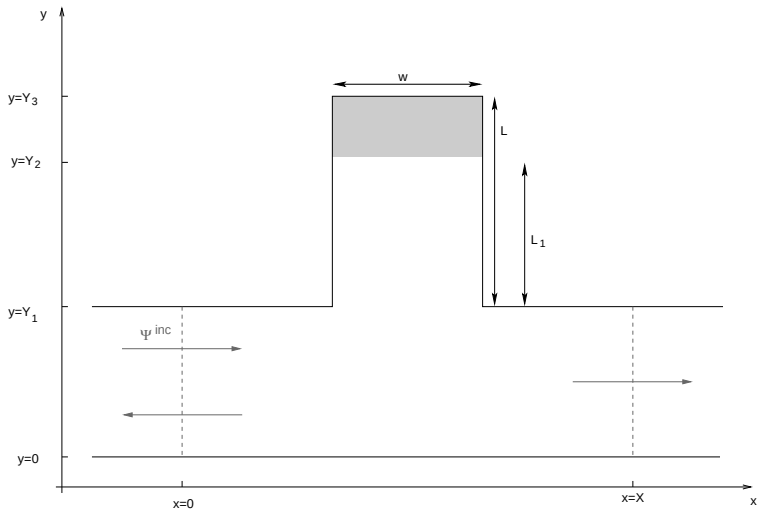

Figure 6: T-shaped structure Ω with the length $X = 60$nm, a channel width $Y_1 = 20$nm, and a stub width $w = 20$nm. It is possible to switch the stub length from $L_1 = 32$nm to $L_2 = 40.5$nm. Inhomogeneous DTBCs are implemented at $x = 0$ and $x = X$, the inflow is modeled by the function ψ^{Inc} given in equation (5.6).

ductor material of Ω. To model a constant inflow of electrons at the device contacts, we use inhomogeneous TBCs. In the 1D case they read (cf. [Ar01])

$$\partial_\eta \left(e^{iV_{ext}t}\psi - \psi^{Inc}\right) = -\sqrt{\frac{2m_*}{\hbar}}e^{-i\pi/4}\sqrt{\partial_t}\left(e^{iV_{ext}t}\psi - \psi^{Inc}\right), \quad x_0 = 0 \text{ or } x_0 = X\,,$$

with the constant external potential V_{ext} and the incoming wave function $\psi^{Inc}(x_0, y, t)$. In 2D this TBC has to be applied to each Fourier mode $\hat{\psi}_m(x, t)$, analogously to the homogeneous case (1.4), cf. [BeMePi05].

In x-direction the channel shown in Figure 6 has a length of $X = 60$nm; the channel width Y_1 and the stub width w are both 20nm. In order to control the current through the channel, the stublength can be changed from $L_1 = 32$nm to $L_2 = 40.5$nm. TBCs are implemented at $x = 0$ and $x = X$. All other boundaries are considered as hard walls, i.e. we use Dirichlet boundary conditions for ψ. Using $V_{ext} = 0$, a time harmonic incoming function

$$\psi^{Inc}(x = 0, y, t) := \sin\left(\frac{y\pi}{Y_1}\right)e^{-\frac{iEt}{\hbar}}, \quad y \in [0, Y_1] \tag{5.6}$$

is modelling the mono-energetic, constant-in-time incoming current at $x = 0$. Here, ψ^{Inc} includes only the lowest y-mode. But any linear combination of higher modes would

work equally well, which is a great advantage compared to other artificial boundary conditions (e.g. [Bu97]). In our example the energy E of the incoming wave equals 29.9meV and the effective electron mass has the value $m_* = 0.067m_0$ (m_0 being the electron mass in vacuum), which corresponds to GaAs.

For the subsequent simulation we solve the Schrödinger equation (5.5) without external potential, i.e. $V = 0$. For realistic simulations of MOSFET-channels (5.5) should be coupled to the self-consistent Coulomb potential inside the channel. Since we focus on DTBCs, we shall not include this here. But a coupling to the Poisson equation *inside* the computation domain does *not* change the derivation or discretization of our open boundary conditions.

In the subsequent simulations we are mostly interested in the switching and the large time behaviour of this waveguide. Therefore we first need to compute a stationary state corresponding to a given incoming plane wave function ψ^{Inc}. To this end we choose the following (somewhat arbitrary) initial function

$$\psi^I(x,y) = \begin{cases} \sin\left(\frac{y\pi}{Y_1}\right) e^{ik_x x} & : \quad 0 \le x < x_1 \\ \frac{1}{2}\sin\left(\frac{y\pi}{Y_1}\right) e^{ik_x x}\left[1+\cos\left(\pi\frac{x-x_1}{x_2-x_1}\right)\right] & : \quad x_1 \le x < x_2 \\ 0 & : \quad x \ge x_2 \end{cases} \tag{5.7}$$

with $x_1 = 5$nm and $x_2 = 15$nm, which is consistent with the incoming wave. Then we solve the transient Schrödinger equation until stationarity.

In the analytical case the dispersion relation for (5.5) on a domain $\mathbb{R} \times (0, Y_1)$ with a plane wave solution in the first orthogonal mode (cf. (5.6)) reads

$$\epsilon(k_x) = \frac{\hbar^2 k_x^2}{2m_*} + \frac{\hbar^2\pi^2}{2m_* Y_1^2}, \tag{5.8}$$

which needs to be modified for the discretized Schrödinger equation. For a given inflow energy E, the value of k_x appearing in (5.7) can be derived from the following *discrete dispersion relation*. To derive it, we first put the ansatz $\psi_{j,1} = e^{ik_x j\Delta x}\sin\left(\frac{\pi\Delta y}{Y_1}\right)$, $j \in \mathbb{Z}$ into the spatial semi-discretization (by the compact nine-point scheme) analogous to (2.5):

$$\begin{aligned} E_{space}(k_x) \;=\; & \Big[-\frac{\hbar^2}{m_*\Delta x^2}\left(\cos(k_x\Delta x)-1\right) - \frac{\hbar^2}{m_*\Delta y^2}\left(\cos\left(\frac{\pi\Delta y}{Y_1}\right)-1\right) \\ & -\frac{\hbar^2(\Delta x^2+\Delta y^2)}{6m_*\Delta x^2\Delta y^2}\left(\cos(k_x\Delta x)-1\right)\left(\cos\left(\frac{\pi\Delta y}{Y_1}\right)-1\right)\Big] \\ & \times\Big[1+\frac{1}{6}\left(\cos(k_x\Delta x)-1\right)+\frac{1}{6}\left(\cos\left(\frac{\pi\Delta y}{Y_1}\right)-1\right)\Big]^{-1}. \end{aligned} \tag{5.9}$$

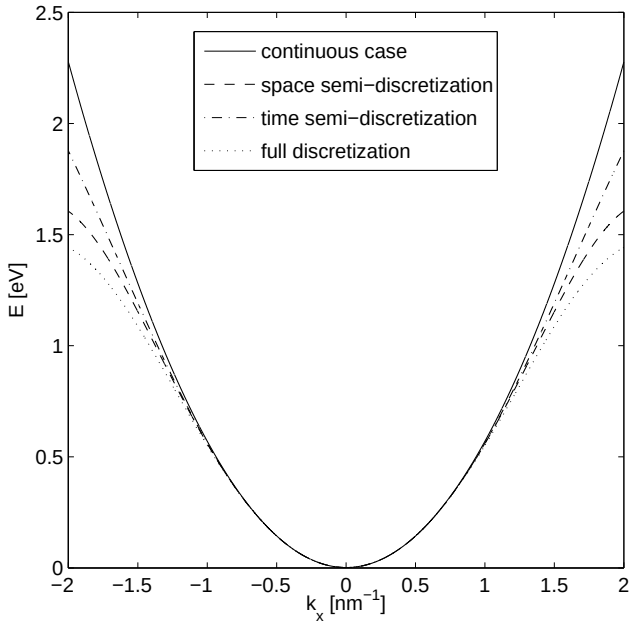

Figure 7: Dispersion relation for the Schrödinger equation (5.5) as a function of the wavenumber k_x for the parameters $\Delta x = 1.44$nm, $\Delta t = 0.5$fs: Continuous case (solid line), space semi-discretization (dashed line), time semi-discretization (dash-dotted line), and full discretization (dotted line).

This is the dispersion relation modified due to the spatial discretization. Adding now the correction due to the Crank-Nicolson time discretization yields the dispersion relation

$$E(k_x) \quad = \quad \frac{\hbar}{i\Delta t} \ln\left(\frac{2i\hbar - \Delta t E_{space}(k_x)}{2i\hbar + \Delta t E_{space}(k_x)}\right) \tag{5.10}$$

for the discrete Schrödinger equation (analogous to (2.5)) with a time-harmonic plane wave solution. Figure 7 shows these different dispersion relations as a function of $k_x \in [-2\text{nm}^{-1}, 2\text{nm}^{-1}]$ for the discretization parameters $\Delta x = 1.44$nm, $\Delta t = 0.5$fs. Only for small values of k_x the continuous (5.8), the time-discretization-corrected, the space-discretization-corrected (5.9), and the fully discrete dispersion relation (5.10) are close to each other. Otherwise corrections due to $E(k_x)$ from (5.10) are necessary.

Numerical tests have shown that the real and imaginary parts of the solution to the Schrödinger equation (5.5) with constant inflow (5.6) are highly oscillatory in time, such that a fine time discretization seems necessary. Figure 8(a) shows the highly oscillatory evolution of the real part at one spatial grid point in the T-shaped structure with constant inflow ψ^{Inc}. For this plot we considered 50 000 time steps with $\Delta t = 0.2$fs, $V = 0$,

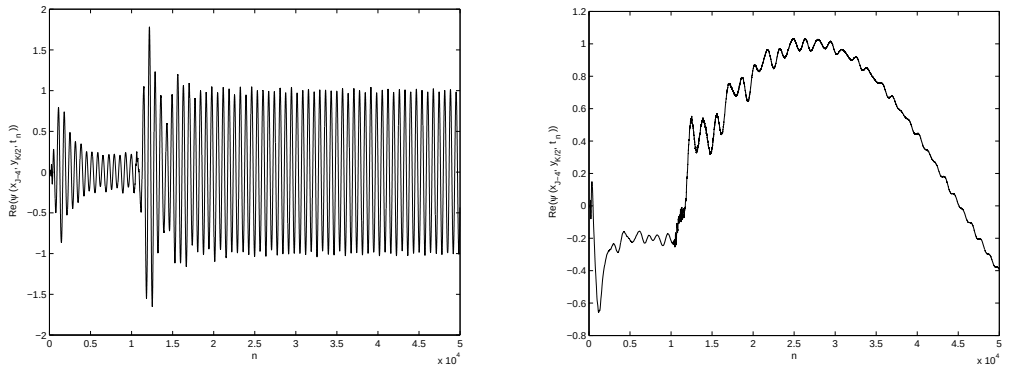

(a) $\mathrm{Re}\,(\psi(x_{J-4}, y_{K/2}, t_n))$ (b) $\mathrm{Re}\,(\varphi(x_{J-4}, y_{K/2}, t_n))$

Figure 8: Time evolution of the real part to the solution of the Schrödinger equation in the T-shaped device at the one grid point $(x_{J-4}, y_{K/2})$. (a) shows $\mathrm{Re}\big(\psi(x_{J-4}, y_{K/2}, t_n)\big)$ for time steps $n = 1, \ldots, 50\,000$ with $V = 0$. (b) shows the evolution of $\mathrm{Re}\big(\varphi(x_{J-4}, y_{K/2}, t_n)\big)$ under the assumption $V = -E$. After 10 000 time steps the stub length is switched from $L_1 = 32$nm to $L_2 = 40.5$nm.

and $\Delta x = \Delta y = 0.5$nm ($J = K = 120$). After 10 000 time steps the stub length is switched from $L_1 = 32$nm to $L_2 = 40.5$nm. In order to use a coarser time discretization (in spite of these oscillations), we consider the simple transformation

$$\varphi(x, y, t) := e^{-i\omega t}\psi(x, y, t), \tag{5.11}$$

with the dominant time frequency $\omega = -\frac{E}{\hbar}$. φ then satisfies the modified Schrödinger equation

$$i\hbar\varphi_t \;=\; -\frac{\hbar^2}{2m_*}\big(\varphi_{xx} + \varphi_{yy}\big) + (V - \omega\hbar)\varphi, \tag{5.12}$$

with $\varphi^I = \psi^I$ and incoming plane wave

$$\varphi^{Inc}(x = 0, y, t) = \sin\left(\frac{y\pi}{Y_1}\right). \tag{5.13}$$

As expected, its solution is much "smoother" in time (cf. Figure 8(b)). Hence, we expect that φ allows for a much more accurate numerical solution. To verify this claim numerically, we discretize both versions of the Schrödinger equation on the fixed time interval $[0, 10\text{ps}]$. ψ_1 is obtained from (5.5) with the parameters $N = 12\,500$, $\Delta t = 0.8$fs and $V = 0$. $\psi_2(t_n) := e^{i\omega t_n}\varphi(t_n)$ is obtained from discretizing (5.12) with the parameters $N = 12\,500$, $\Delta t = 0.8$fs, and $V = -E$. As an even more accurate reference solution we

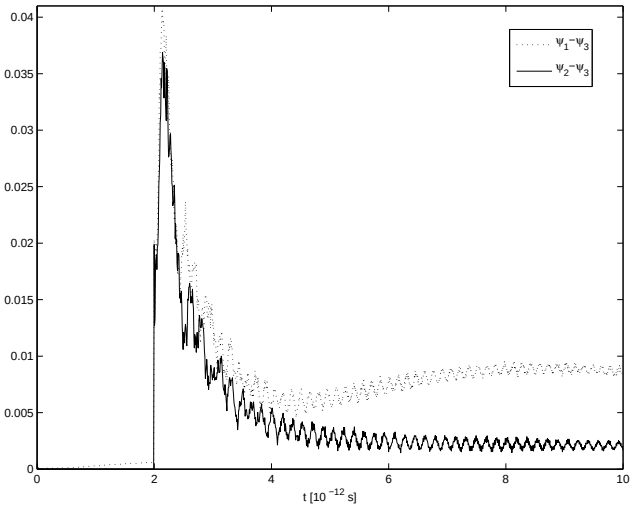

Figure 9: Time evolution of the spatial ℓ^2-error of ψ_1 and ψ_2 w.r.t. the reference solution ψ_3; $\cdots\cdots$ $||\psi_1(t_n) - \psi_3(t_n)||_2$; ——— $||\psi_2(t_n) - \psi_3(t_n)||_2$.

use $\psi_3(t_n) := e^{i\omega t_n}\varphi(t_n)$ with the parameters $N = 100\,000$, $\Delta t = 0.1$fs, and $V = -E$. In Figure 9 we show the evolution of the spatial error-norms $||\psi_1(.,.,t_n) - \psi_3(.,.,t_{8n})||_2$ and $||\psi_2(.,.,t_n) - \psi_3(.,.,t_{8n})||_2$ for the time steps $n = 0, \ldots, 12\,500$. At the time $T = 2$ps we switched the stub length from $L_1 = 32$nm to $L_2 = 40.5$nm. As expected, the function ψ_2 is more accurate than function ψ_1 with respect to the function ψ_3. Therefore, the transformed equation (5.12) shall be used for the subsequent simulations.

Figure 10 shows some temporal snapshots of the solution to the modified Schrödinger equation (5.12). And Figure 11 shows the corresponding longitudinal current density

$$j(x,t) = \int_0^{Y_3} J_x(x,y,t)dy, \tag{5.14}$$

where the x-component of the current density is defined as

$$J_x(x,y,t) = \frac{\hbar}{2m_*}\mathrm{Im}\left(\psi(x,y,t)\frac{\partial}{\partial x}\bar{\psi}(x,y,t)\right).$$

In this simulation the stub length is first fixed to $L_1 = 32$nm. After about 2ps the solution reaches a steady state and the current inside the device is already almost constant in x at the low value $0.03\text{nm}^2/\text{ps}$ ("off-state" of the waveguide, cf. 11(c)).

Phenomenologically speaking, in this case only $1\frac{1}{2}$ wave packets "fit" into the stub (cf. Figure 10(c)). Hence, they block the current flow through the waveguide. Then, at $t = 2$ps the stub is enlarged at once to $L_2 = 40.5$nm. After some transient phase, the solution converges to another steady state ("on-state" of the waveguide, cf. Figure 10(f), 11(f)). Here two wave packets "fit" into the stub. Hence, the current can flow almost unblocked through the device, so that the current is reaching an almost constant maximum level. Note that for a two-dimensional channel of width 20nm (same as for the T-shaped geometry), but without any barriers and stubs, and for the given inflow energy $E = 29.9$meV, the constant "free" current $j(x,t)$ equals $0.4\text{nm}^2/\text{ps}$.

6 Conclusion

We have generalized the fourth order "Numerov" finite difference scheme to the transient 2D Schrödinger equation and derived the corresponding *discrete transparent boundary conditions*. Its numerical efficiency is demonstrated in numerical tests on a rectangular geometry as well as for quantum waveguide simulations.

Acknowledgment: The authors acknowledge stimulating discussions with Olivier Vanbesien on waveguide simulations. The second author (A.A.) was partly supported be the DFG-project no. AR 277/3-3 and the Wissenschaftskolleg *Differentialgleichungen* of the FWF.

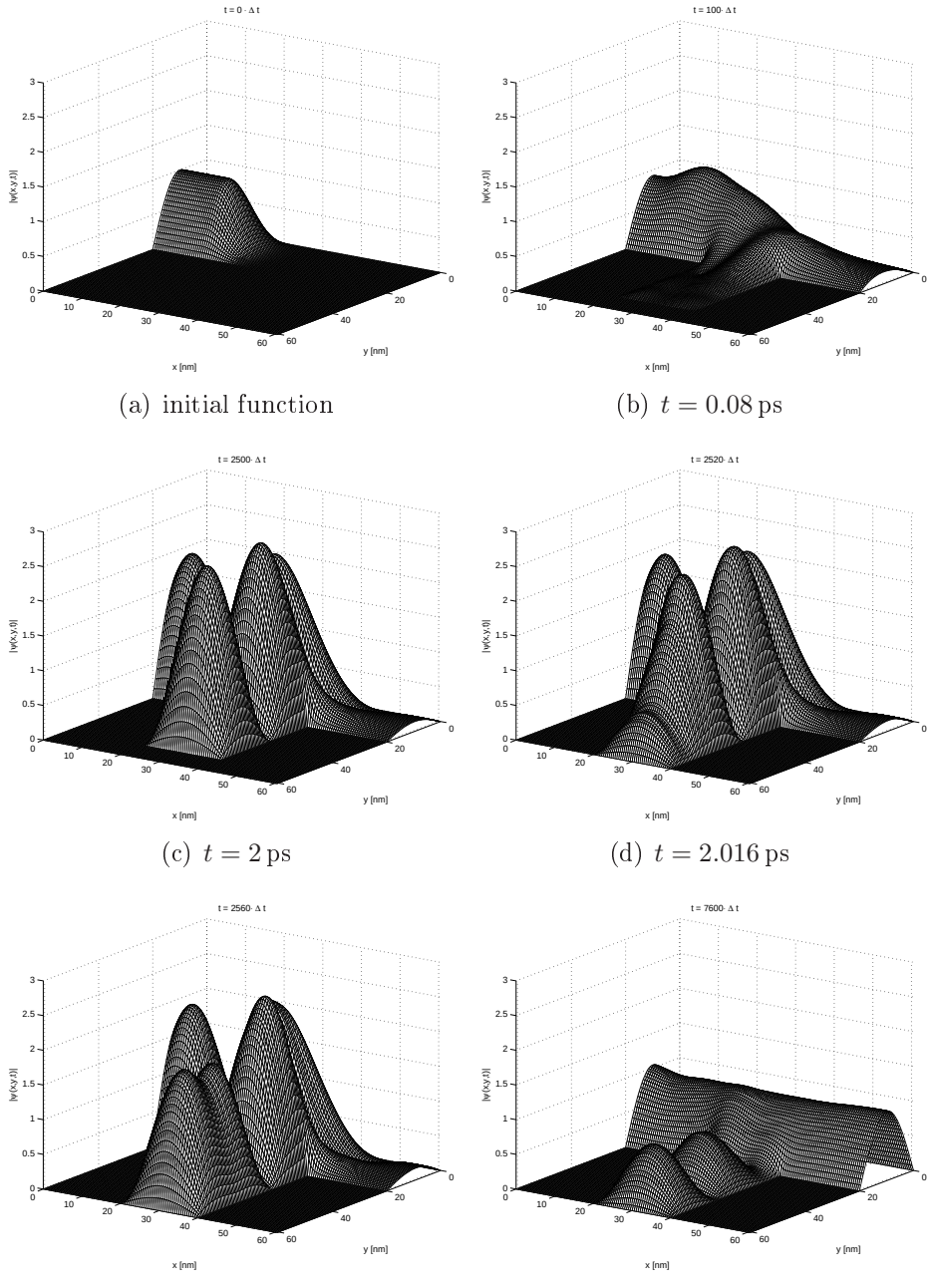

(a) initial function (b) $t = 0.08\,\mathrm{ps}$

(c) $t = 2\,\mathrm{ps}$ (d) $t = 2.016\,\mathrm{ps}$

(e) $t = 2.048\,\mathrm{ps}$ (f) $t = 6.08\,\mathrm{ps}$

Figure 10: Absolute value of the solution $\psi(x, y, t)$ of the time-dependent Schrödinger equation (5.5) on the T-shaped structure from Figure 6. The discretization parameters are $\Delta x = \Delta y = 0.25\mathrm{nm}$, $\Delta t = 0.8\mathrm{fs}$, $V = -E = -29.9\mathrm{meV}$, $m_* = 0.067 m_0$. (c) shows the steady state corresponding to the short stub with $L_1 = 32\mathrm{nm}$. (f) is the steady state for the long stub with $L = 40.5\mathrm{nm}$.

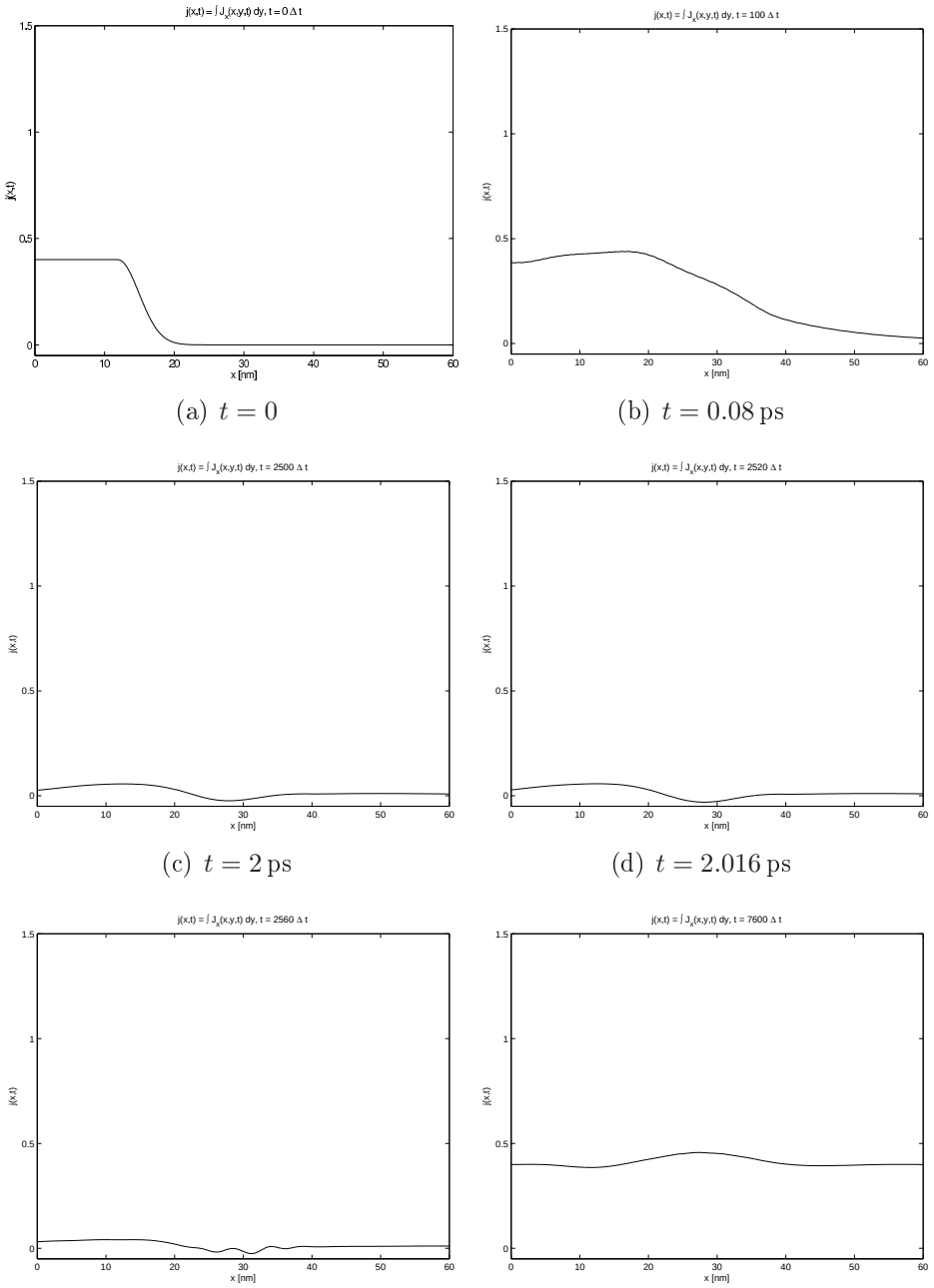

(a) $t = 0$ (b) $t = 0.08\,\mathrm{ps}$

(c) $t = 2\,\mathrm{ps}$ (d) $t = 2.016\,\mathrm{ps}$

(e) $t = 2.048\,\mathrm{ps}$ (f) $t = 6.08\,\mathrm{ps}$

Figure 11: Current density $j(x,t)$ (in $\mathrm{nm}^2/\mathrm{ps}$) in the T-shaped device for the same example as in Figure 10. In (c) and (f) the current is (almost) constant in x – a requirement for a steady state.

References

[AiYaMi93] K. Aihara, M. Yamamoto, T. Mizutani: *Three-terminal conductance modulation of a quantum interference device using a quantum wire with a stub structure*, Appl. Phys. Lett. 63 (1993) 3595-3597

[AlRe02] I. Alonso-Mallo, N. Reguera: *Weak ill-posedness of spatial discretizations of absorbing boundary conditions for Schrödinger-type equations*, SIAM J. Numer. Anal. 40 (2002) 134-158

[AlRe03] I. Alonso-Mallo, N. Reguera: *Discrete absorbing boundary conditions for Schrödinger-type equations, construction and error analysis*, SIAM J. Numer. Anal. **41** (2003), 1824-1850

[AlRe04] I. Alonso-Mallo, N. Reguera: *Discrete Absorbing Boundary Conditions for Schrödinger-type equations. Practical Implementation*, Math. Comp. 73 (2004) 127-142

[AABES07] X. Antoine, A. Arnold, C. Besse, M. Ehrhardt, A. Schädle: *A Review of Transparent and Artificial Boundary Conditions Techniques for Linear and Nonlinear Schrödinger Equations*, submitted to Appl. Numer. Math. 2007.

[AnBe01] X. Antoine, C. Besse: *Construction, structure and asymptotic approximations of a microdifferential transparent boundary condition for the linear Schrödinger equation*, J. Math. Pures Appl. (9) 80 (2001) 701-738

[AnBeMo04] X. Antoine, C. Besse, V. Mouysset: *Numerical schemes for the simulation of the two-dimensional Schrödinger equation using non-reflecting boundary conditions*, Math. Comp. 73, no. 248 (2004), 1779-1799

[ASSHFLL96] J. Appenzeller, C. Schroer, T. Schäpers, A. v.d. Hart, A. Förster, B. Lengler, H. Lüth: *Electron interference in a T-shaped quantum transistor based on Schottky-gate technology*, Phys. Rev. B 53, no. 15 (1996) 9959-9963

[Ar98] A. Arnold: *Numerically absorbing boundary conditions for quantum evolution equations*, VLSI Design 6, no. 1-4 (1998) 313-319

[Ar01] A. Arnold: *Mathematical concepts of open quantum boundary conditions*, Transp. Theory Stat. Phys. 30, no. 4-6 (2001) 561-584

[ArEhSo03] A. Arnold, M. Ehrhardt, I. Sofronov: *Approximation, stability and fast calculation of non-local boundary conditions for the Schrödinger equation*, Commun. Mathematical Sciences 1, no. 3 (2003) 501-556

[AvKoSi00] G. Avdelas, A. Konguetsof, T.E. Simos: *A generalization of Numerov's method for the numerical solution of the Schrödinger equation in two dimensions*, Computers and Chemistry 24 (2000) 577-584

[BaPo91] V.A. Basakov, A. V. Popov: *Implementation of transparent boundaries for numerical solution of the Schrödinger equation*, Wave Motion 14 (1991) 123-128

[BaShMa02] W. Bao, J. Shi, P.A. Markowich: *On time-splitting spectral approximation for the Schrödinger equation in the semiclassical regime*, J. Comput. Phys. 175, no. 2 (2002) 487-524

[BeMePi05] N. Ben Abdallah, F. Méhats, O. Pinaud: *On an open transient Schrödinger-Poisson system*, Math. Models Methods Appl. Sci. 15, no. 5 (2005) 667-688

[BoDe06] A. Borzi, E. Decker: *Analysis of a leap-frog pseudospectral scheme for the Schrödinger equation*, J. Comp. Appl. Math. 193, no. 1 (2006) 65–88

[Bu97] L. Burgnies: *Mecanismes de conduction en regime ballistique dans les dispositifs electroniques quantiques*, Ph. D. thesis, Université des Sciences et Technologies de Lille (1997)

[Co66] L. Collatz: *The numerical treatment of differential equations*, Springer Verlag (1966)

[Do51] H. Doerrie: *Unendliche Reihen*, Oldenbourg Verlag (1951)

[EhAr01] M. Ehrhardt, A. Arnold: *Discrete Transparent Boundary Conditions for the Schrödinger Equation*, Revista di Matematica della Universita di Parma 6, no. 4 (2001) 57-108

[EnMa77] B. Engquist, A. Majda: *Absorbing boundary conditions for the numerical simulation of waves*, Math. Comp. 31 (1977) 629-651

[EnMa79] B. Engquist, A. Majda: *Radiation boundary conditions for acoustic and elastic wave calculations* Comm. Pure Appl. Math. 32 (1979) 314-358

[Fe99] T. Fevens, H. Jiang: *Absorbing boundary conditions for the Schrödinger equation*, SIAM J. Sci. Comp. 21, no. 1 (1999) 255-282

[HePfSt07] B. Heubeck, C. Pflaum, G. Steinle: *New Finite Elements for Large-Scale Simulation of Optical Waves*, Preprint (2007)

[JiLu02] G. Jing, M.S. Lundstrom: *A computational study of thin-body, double-gate, Schottky barrier MOSFETs*, IEEE Tran. on Elec. Dev. 49, no. 11 (2002) 1897-1902

[KaMoSi05] Z. Kalogiratou, T. Monovasilis, T. E. Simos: *Numerical solution of the two-dimensional time independent Schrödinger equation with Numerov-type methods*, J. Math. Chem. 37, no. 3 (2005) 271-279

[KoKo86] R. Kosloff, D. Kosloff: *Absorbing boundaries for wave propagation problems*, J. Comp. Phys. 63 (1986) 363-376

[Ku92] J.-P. Kuska: *Absorbing boundary conditions for the Schrödinger equation on finite intervals*, Physical Review B 46, no. 8 (1992) 5000-5003

[Ma89] B. Mayfield: *Non-local boundary conditions for the Schrödinger equation*, Ph. D. thesis, University Rhode Island, Providence, RI (1989)

[Mo04] C.A. Moyer: *Numerov extension of transparent boundary conditions for the Schrödinger equation in one dimension*, Am. J. Phys. 72, no. 3 (2004) 351-358

[Mo06] C.A. Moyer: *Numerical Solution of the Stationary State Schrödinger Equation Using Discrete Transparent Boundary Conditions*, Computing in Science and Engineering 8, no. 4 (2006) 32-40

[NeBa89] D. Neuhauser, M. Baer: *The time-dependent Schrödinger equation: Application of absorbing boundary conditions*, J. Chem. Phys. 90, no. 8 (1989) 4351-4355

[Pa82] J. S. Papadakis: *Impendance formulation of the bottom boundary condition for the parabolic equation model in underwater acoustics*, NORDA Parabolic Equation Workshop, NORDA Tech. Note 143 (1982)

[Ra02] L. Ramdas Ram-Mohan: *Finite element and boundary element applications in quantum mechanics*, Oxford Univ. Press, (2002)

[Sc02] A. Schädle: *Non-reflecting boundary conditions for the two dimensional Schrödinger equation*, Wave Motion 35 (2002) 181-188

[Sh91] T. Shibata: *Absorbing boundary conditions for the finite-difference time-domain calculation of the one-dimensional Schrödinger equation*, Physical Review B 43, no. 8 (1991) 6760-6763

[St04] J. C. Strikwerda: *Finite Difference Schemes And Partial Differential Equations*, Society for Industrial and Applied Mathematics (2004)

[StBu90] J. Stoer, R. Bulirsch: *Numerische Mathematik 2*, Springer Verlag (1990)

[Sz04A] J. Szeftel: *Design of Absorbing Boundary Conditions for Schrödinger equations in* $\mathbb{R}^d$, SIAM J. Numer. Anal. 42, no. 4 (2004) 1527-1551

[Sz04B] J. Szeftel: *Refléxion des singularités pour l'équation de Schrödinger*, Comm. Partial Differential Equations 29, no. 5-6 (2004) 707-761

[Sz75] G. Szegö: *Orthogonal Polynomials*, Vol XXIII AMS, 4th ed. (1975)

[WaPoLu04] J. Wang, E. Polizzi, M. Lundstrom: *A Three-Dimensional Quantum Simulation of Silicon Nanowire Transistors with the Effective-Mass Approximation*, J. Appl. Phys. 96, no. 4 (2004), 2192-2203